

Detection of shear due to weak lensing by large-scale structure

P. Schneider¹, L. van Waerbeke^{1,4}, Y. Mellier^{2,3},
B. Jain¹, S. Seitz¹ & B. Fort³

¹ Max-Planck-Institut für Astrophysik, Postfach 1523, D-85740 Garching, Germany,

² Institut d'Astrophysique de Paris, 98 bis boulevard Arago, F-75014 Paris, France,

³ DEMIRM, Observatoire de Paris, 61 Avenue de l'Observatoire, F-75014 Paris, France,

⁴ Observatoire Midi-Pyrénées, 14 Avenue Edouard Belin, F-31400 Toulouse, France,

Abstract

We present evidence for a coherent shear signal in a field containing the $z = 1.2$ radio-source PKS1508-05. Since there were no intervening mass concentrations known before targeting this field, we interpret this signal as due to weak lensing by large-scale structure. This result is the outcome of a re-analysis of the observations of Fort et al. (1996) in the fields of three high redshift QSO/radio-sources. Several tests of the robustness of the signal were performed: subdivision of the field and tests using simulated data with randomized ellipticity orientation; using the pixel-to-pixel autocorrelation function method to measure the shear; using the correlation function of the galaxy ellipticities with bootstrap resampling to estimate errors and to find the typical angular separation that dominates the signal. We find that the field of PKS1508-05 contains a robust shear signal that is coherent over the $2'$ by $2'$ field. The signal is detected at a high level of significance ($\gtrsim 99.6\%$) using the tests described above. The amplitude of the shear on a scale of $1'$ is about 3%, which is consistent with theoretical expectations from weak lensing by large-scale structure.

1. Introduction

Weak gravitational lensing has found its main application up to now in reconstructing the projected surface mass density in massive clusters of galaxies (e.g., Kaiser & Squires 1993; Fahlman et al. 1994; Seitz et al. 1996; Squires et al. 1996; for recent reviews, see Fort & Mellier 1994; Schneider 1996; Narayan & Bartelmann 1996). Blandford et al. (1991), Kaiser (1992, 1996), Miralda-Escude (1991), Villumsen (1996a) and others considered the shear signal caused by the tidal field of the large-scale matter distribution in the universe. The two-point correlation function of the observable shear, for example, can be directly written in terms of the power spectrum of the cosmological density fluctuations. These investigations, which are mainly based on the linear theory of the evolution of density fluctuations, concluded that the rms of the expected shear is of the order of one percent, depending on the cosmological model, the normalization of the power spectrum, and the assumed redshift distribution of the faint galaxies.

Since the expected signal is so small, it is evident that this so-called cosmic shear will be difficult to observe with ground-based telescopes – the anisotropy of the PSF and the instrumental image distortions have to be understood to a percent level in order to exclude systematic effects. The observational study by Mould et al. (1994) did not find a shear signal and put an upper limit on the shear in their field of $\sim 4\%$, though a later reanalysis of the same data by Villumsen (1996b) yielded a detection with large formal significance. Such investigations push the instruments and the telescopes to the limits of their capabilities and ideally they should be done preferably with the HST. Unfortunately, this is prohibitively difficult due the small field-of-view of the current generation of its instruments.

Recently, progress in the theoretical predictions has been made by dropping the approximation of linear density growth. Bernardeau, Van Waerbeke & Mellier (1996) have calculated the skewness of the magnification in the weakly non-linear regime, and Jain & Seljak (1996) have calculated the rms of the mean cosmic shear and its two-point correlation function using the fully non-linear evolution of the dark matter power spectrum. The latter study showed that on scales below ~ 20 arcmin the cosmic shear is significantly larger than estimated from linear density growth, a trend already hinted at in the numerical simulations presented in Blandford et al. (1991). These new results are encouraging, and suggest that the detection of cosmic shear with ground-based telescopes should be more feasible on small scales.

In this paper we re-analyze the observations of Fort et al. (1996; hereafter FMDBK) of image distortions of faint galaxies around high-redshift QSOs. The goal of their study was to test the hypothesis initially proposed by Bartelmann & Schneider (1992) that the observed association of high-redshift QSOs with foreground galaxies on arcminute scales (e.g., Tyson 1986; Fugmann 1990; Bartelmann & Schneider 1994; Benítez & Martínez-González 1997, and references therein) is caused by lensing by large-scale matter inhomogeneities in which the galaxies are embedded (Bartelmann 1995). Surprisingly, FMDBK found a significant shear signal around several of the observed QSOs; they demonstrated that this shear signal is considerably stronger than the instrumental image distortion and the anisotropy of the PSF. Their results were confirmed at least for the quasar 3C 336 (referenced as Q1622 in FMDBK) from analyses of HST images (Bower & Smail 1997), which gives good confidence that the signal detected by FMDBK is real and significant.

In this paper, we argue that FMDBK have detected a cosmic shear signal — though

along biased lines-of-sight, if the magnification bias hypothesis for the high-redshift QSOs is correct. In Sect. 2 we briefly summarize the observations and the results of FMDBK. The shear measurements are then analyzed in Sect. 3, by comparing them with those obtained from randomizing the orientation angles of the faint (background) galaxies, thus determining the significance of the measured shear. In particular it will be shown, by considering the measured ellipticity of stars in the fields observed with the SUSI camera at the ESO NTT, that the anisotropy of the PSF is well below 1% and thus does not cause a spurious shear signal. One of the fields, that around the QSO PKS1508–05, exhibits a very strong and nearly uniform shear across the whole SUSI field ($\sim 2' \times 2'$). In Sect. 4, we present further evidence for this shear, by calculating the pixel-to-pixel auto-correlation function (ACF) of the image, using different cuts for the brighter images which are excluded in this ACF, thus following the method introduced by van Waerbeke et al. (1997). This provides good confidence that the shear detected is not an artefact which results from the specific technique we use to measure the galaxy ellipticity. Finally, a different measure for the shear is obtained from the two-point correlation function of galaxy ellipticities; this is constructed in Sect. 5 and its statistical significance is tested both with bootstrapping methods as well as with randomizations of position angles. Our results are discussed in Sect. 6.

2. Observations and previous results

The five QSO fields in FMDBK were selected on the basis of their high radio and optical luminosity. This selection was designed to test the hypothesis that such QSOs are magnification biased by intervening large-scale matter inhomogeneities. Four of these QSO fields were observed with the SUSI camera at the ESO New Technology Telescope at La Silla, and one was observed with FOCAM (3C 336) at the Canada-France-Hawaii-Telescope (CFHT) on Mauna Kea. For details of the observing runs, see FMDBK.

The field of PKS1741–03 was chosen for studying the instrumental distortion properties of SUSI; it is crowded by stars and has been used in FMDBK to demonstrate the remarkable stability of the PSF across the SUSI field.

The QSO 3C 336 was observed at CFHT and shows a strong shear signal. A deep WFPC2 image from the Hubble Space Telescope and extensive spectroscopy of galaxies in the field (Steidel et al. 1996) has shown that the distribution of galaxies spans a wide range in redshift; in fact, the QSO itself appears to reside in a cluster. It is therefore unclear whether the observed shear, whose presence was confirmed from the HST image (M. Dickinson, private communication; Bower & Smail 1997) is due to material in the foreground of the QSO, which is therefore able to magnify it, or due to a mass overdensity surrounding the QSO. The latter possibility would be no less exciting than the first and would add another high-redshift cluster to the list of those which are strong enough for a shear detection (see Luppino & Kaiser 1997; G. Luppino, private communication), implying either that a substantial fraction of the population of faint galaxies are at redshifts well beyond one, or that clusters at redshift $z \sim 0.8 - 1$ are very massive, contradicting predictions made in some cosmogonic models, or both.

Since the stability of the PSF across the SUSI field allows us to estimate the significance of a measured shear without correcting for an anisotropic PSF component (e.g., Kaiser, Squires & Broadhurst 1995), we shall concentrate in this paper on the three QSO

fields PKS0135–247, PKS1508–05 and 3C446. The seeing in these fields ranges from 0''.66 to 0''.76, and the total exposure time from 13500s to 19700s in the V band. For each QSO field we obtained two catalogues of objects. One was constructed using the same method as described in Bonnet & Mellier (1995), where the object detection is performed using a standard detection algorithm similar to FOCAS, and the ellipticity of the images is measured by a weighted second-order moment scheme. We refer to the corresponding ellipticities as ‘Bonnet/Mellier (or BM) ellipticities’. A second catalog was constructed using the SExtractor software package (Bertin 1996, Bertin & Arnouts 1996). These ellipticities are determined from second moments calculated within a fixed limiting isophote of the objects and will be referred to as ‘S-ellipticities’. Only objects with $\text{flag} \leq 4$ and $\text{size} \geq 8$ pixels are included in the S-catalog. The final object catalogues consist of ($N_{\text{BM}} = 148/N_{\text{S}} = 148$) objects for 0135, (145/144) for 1508, and (211/143) for 3C446.

From the S-catalog, we obtained a list of stellar candidates. Each of these was carefully checked by eye and removed from the list of stellar objects if they were saturated, not isolated, too faint, or appeared non-stellar by eye-inspection. The remaining list of ‘good’ stars contained 4, 5 and 7 objects for 0135, 1508 and 3C446, respectively. Their ellipticities are plotted in Figs. 1 through 3. We have not attempted here to measure the ellipticity of stars with the BM-method because this method is designed to avoid as much as possible the influence of the PSF.

The BM-ellipticities have smaller values than the ellipticities measured by SExtractor (or any standard algorithms), as was noted in Bonnet & Mellier (1995); this is due to the particular weighting function employed by BM, specifically designed to avoid the core of the PSF. There, a simulated image was analyzed, with a known value of the applied shear and with the same samplings and seeings as the CFHT and NTT images. The ratio of the mean ellipticity in this image (adopted to a deep CFHT image of the cluster CL 0024+16) to the true value of the shear was found to be ~ 6 . On the other hand, Wilson, Cole & Frenk (1996) have performed similar simulations using FOCAS ellipticities, and they found a typical ratio of ~ 1.5 between mean ellipticity and true shear for seeing conditions which apply to the images investigated here.

In order to relate BM-ellipticities to S-ellipticities, we have calculated for each of the three QSO fields a complex relative correction factor C , defined such as to minimize

$$\sum_{i=1}^N |\epsilon_i^{\text{S}} - C\epsilon_i^{\text{BM}}|^2, \quad (1)$$

where the sum extends over all objects which are contained in both catalogues (with a maximum positional difference of 2 pixels or 0''.26) and ϵ^{S} and ϵ^{BM} are the complex ellipticities [defined such that for an image with elliptical isophotes of axis ratio $r \leq 1$, $|\epsilon| = (1-r)/(1+r)$]. Ideally, the resulting value of C should have a very small imaginary part. We find for the three fields: $C = 3.17 - 0.36i$ for 0135, $C = 3.36 - 0.29i$ for 1508, and $C = 2.93 + 0.17i$ for 3C446. We note, however, that the precise values of C depend fairly sensitively on cuts applied to the S-catalog. From simulations (van Waerbeke 1997) it became evident that the SExtractor ellipticities depend on the parameters selected for the detection prior to run SExtractor. Since the choice of these parameters are to some degree arbitrary, they are less useful to us for measuring shear on very faint galaxy images than the BM algorithm. This simply reflects that, contrary to BM, SExtractor was not

constructed for measuring such small distortions and should therefore not be used on ground-based images such as those at hand (Bertin, private communication). In the following, we will exclusively use the BM-ellipticities for the very faint galaxies; however, to plot the mean ellipticities from the BM method on the same graph as the ellipticities of stars as measured by SExtractor, we will multiply in these plots the value of $\langle \epsilon^{\text{BM}} \rangle$ by the real part of C . Note that this restriction in the use of SExtractor does not apply to section 4 since for the ACF the very faint galaxies present in the fields are not used.

3. The significance of the shear

The main purpose of this paper is to investigate the statistical significance of the detection of shear in the field of the three QSOs. As discussed below, it is more difficult to determine and interpret the precise value of the shear.

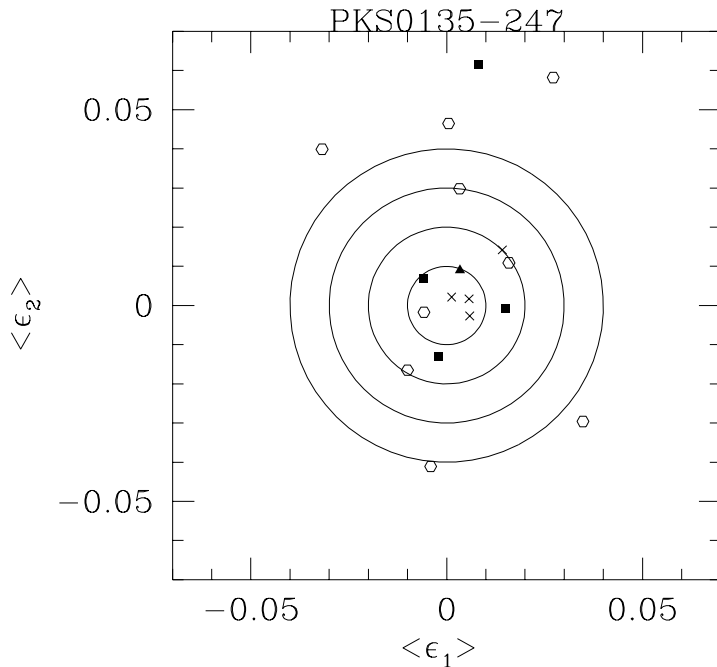


Fig. 1. For the field of the QSO PKS0135–247, the mean ellipticity evaluated over the whole field (solid triangle), over the four subfields with sidelength 1/2 that of the whole field (solid squares), and over the nine subfields with sidelength 1/3 of the whole field (open hexagons) are plotted. The mean ellipticity is obtained from the BM-ellipticity, multiplied by the real part of the correction factor C in order to allow a comparison with the ellipticity of the stars (crosses) measured by SExtractor. Circles of constant $|\epsilon|$ are plotted to guide the eye

In order to test whether the mean ellipticity of images in a (sub)field is statistically significant, we have performed simulations by randomizing the position angles of all objects and measuring the mean ellipticity of these randomized images. For each of the three QSO fields, 10^4 such randomized realizations were conducted. For a given (sub)field, the fraction f of randomized realizations was then determined in which the

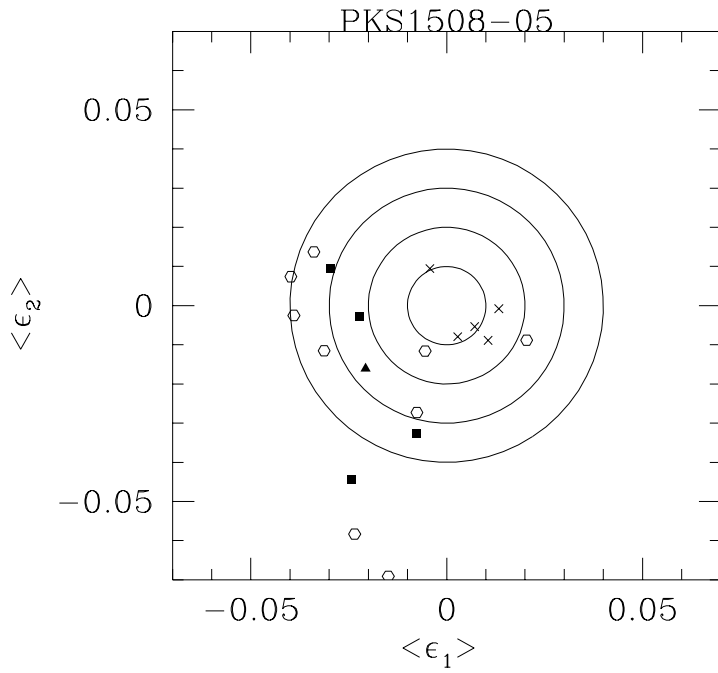


Fig. 2. Same as Fig. 1, for the field of QSO PKS1508-05

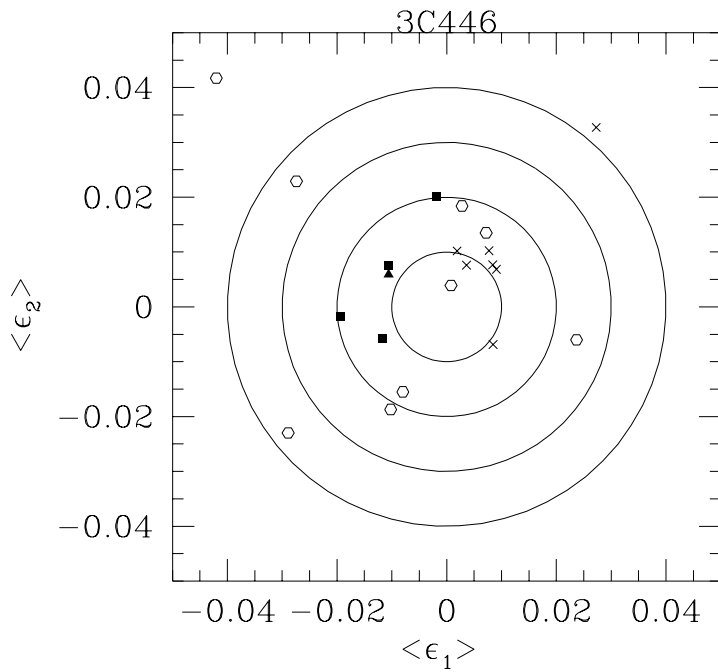


Fig. 3. Same as Fig. 1, for the field of QSO 3C446

absolute value of the mean image ellipticity thus obtained is larger than the mean ellip-

ticity measured from the data. Therefore, f is the probability that the measured mean shear is obtained from a random distribution of image ellipticities with the same amplitudes as the observed images. Small values of f indicate that the observed mean shear is very unlikely to be caused by a random alignment of galaxy images. We shall call f the error level henceforth.

For each QSO field, we have calculated f for the whole field (denoted ‘T’), the four subfields obtained by deviding the total field into four equally sized squares (denoted ‘A’ – lower left, ‘B’ – upper left, ‘C’ – lower right, ‘D’ – upper right, in the frames shown in FMDBK), and the nine subfields obtained by dividing the field into nine equally sized squares, denoted ‘1’ – ‘9’, with the following configuration

$$\begin{pmatrix} 3 & 6 & 9 \\ 2 & 5 & 8 \\ 1 & 4 & 7 \end{pmatrix}.$$

The corresponding values of f are listed in Tables 1 – 3 for each of these (sub)fields, together with the corresponding number N of objects in these fields and the mean ellipticity, which is the BM-ellipticity multiplied by the real part of the correction factor C . Note that the error level f is independent of any scaling of ϵ .

From the values in the tables it is clear that the field around QSO 1508 shows the clearest sign of significant shear, whereas for the two other QSO fields, the evidence for a statistically significant shear is considerably weaker. The shear seems to be quite homogeneous across the field of QSO 1508, and the error level is estimated to be only $\sim 0.2\%$. In addition, for three of the four subfields of sidelength $1/2$ that of the whole field, the error level is well below 10% . In the field of QSO 0135, only two subfields achieve error levels below 3% , and only one subfield in 3C446 is statistically significant, though with an error level of $\sim 0.5\%$. Note that the error level does not strictly correlate with the measured value of $|\langle\epsilon\rangle|$; the number N of galaxies per subfield and their ellipticity distribution are decisive factors in the determination of the statistical significance.

In order to see whether the measured ellipticities are affected by an anisotropic contribution to the PSF, we have plotted the mean values of the ellipticities as given in the tables, together with the measured ellipticity of the stars in each field in Figs. 1 – 3. As can be clearly seen in these figures, the ellipticities of most stars are very similar, and those stars for which ϵ is significantly different from the rest are probably not isolated stars but are contaminated by a nearby or underlying object too faint to be discovered by eye. In addition it should be noted that the mean ellipticity of stars lies in a direction different from the mean ellipticity of galaxies in the fields with smallest error levels – see in particular Fig. 2. We can thus safely exclude the possibility that the high statistical significance obtained in some (sub)fields is due to an anisotropic PSF.

Whereas the evidence for significant shear in the whole field of 3C446 and PKS 0135 is weak, there are nevertheless some subfields around these QSOs where significant shear is detected. As an example, we consider subfield ‘6’ in 3C446, where the error level for the shear detection is a mere 0.5% . In Fig. 4, we have plotted the BM-ellipticities, multiplied by the real part of the correction factor C , of the 26 galaxies in this subfield, together with the 7 stars in this field. The statistically significant shear can be seen by eye, the ellipticities are concentrated towards the upper left corner of the diagram, and it is easily seen that the mean shear in this subfield, as well as the statistical significance, is not dominated by one or two galaxy images. We have checked this quantitatively, by

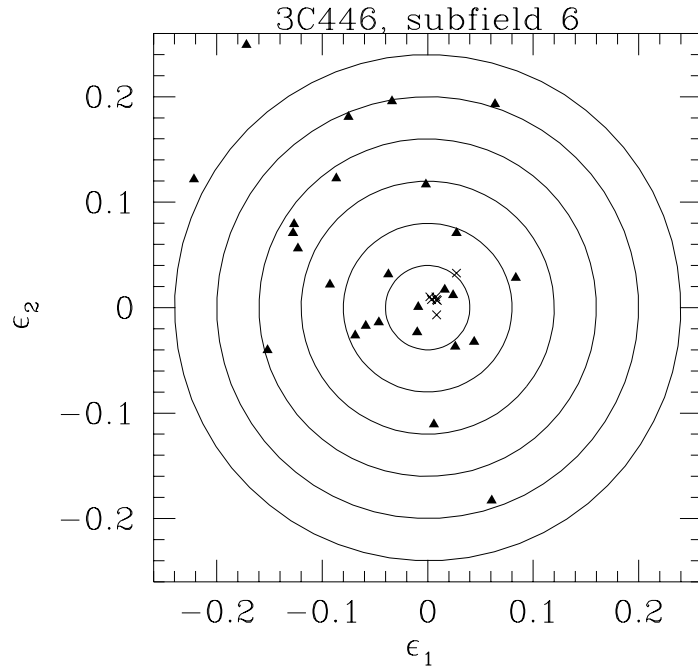


Fig. 4. For the subfield 6 in the field of 3C446, the BM-ellipticities multiplied by the real part of the correction factor C are plotted, together with the SExtractor ellipticities of the seven stars in this field. The anisotropic distribution leading to a significant mean ellipticity in this field is easily seen

removing the two galaxies with largest ellipticities; the resulting value of the error level does not change significantly.

Table 1. For the QSO 0135 and each (sub)field as described in the text, the number N of objects, the error level f , and the measured mean BM-ellipticity, multiplied by the real part of the correction factor (see text) are given

(Sub)field	N	f (in %)	ϵ_1 (in %)	ϵ_2 (in %)
T	148	46.47	0.34	0.90
A	38	83.26	-0.58	0.69
B	40	39.44	1.49	-0.08
C	43	69.95	-0.22	-1.29
D	27	2.38	0.82	6.16
1	14	25.30	-3.18	3.99
2	21	45.31	1.59	1.09
3	16	60.32	-1.00	-1.65
4	33	93.39	-0.58	-0.17
5	12	49.99	0.33	2.98
6	18	2.28	2.72	5.82
7	14	26.39	3.48	-2.96
8	12	36.37	-0.41	-4.11
9	8	58.69	0.05	4.65

Table 2. Same as Table 1, for the QSO 1508

(Sub)field	N	f (in %)	ϵ_1 (in %)	ϵ_2 (in %)
T	145	0.22	-2.07	-1.61
A	37	4.80	-2.96	0.94
B	40	30.06	-2.22	-0.27
C	30	3.85	-2.42	-4.44
D	38	6.44	-0.77	-3.25
1	15	30.52	-3.13	-1.15
2	22	2.65	-3.98	0.74
3	15	36.36	-3.90	-0.25
4	18	25.12	-3.39	1.37
5	15	80.02	-0.55	-1.16
6	15	49.24	2.04	-0.88
7	12	14.84	-1.49	-6.91
8	16	2.41	-2.35	-5.83
9	17	60.90	-0.76	-2.73

Table 3. Same as Table 1, for the QSO 3C446

(Sub)field	N	f (in %)	ϵ_1 (in %)	ϵ_2 (in %)
T	211	20.59	-1.06	0.59
A	64	48.39	-1.06	0.75
B	50	47.01	-1.93	-0.18
C	55	37.22	-0.19	2.02
D	42	67.18	-1.17	-0.58
1	32	53.31	0.28	1.84
2	31	11.36	-2.89	-2.30
3	12	80.48	2.37	-0.60
4	33	64.08	0.72	1.35
5	23	66.12	-0.80	-1.55
6	26	0.52	-4.20	4.17
7	20	40.92	-2.74	2.29
8	20	98.73	0.08	0.39
9	14	69.63	-1.02	-1.87

4. Shear measurement with the ACF

We used the ACF independently on the same images but with somewhat different selection criteria for the galaxies than those used with BM. As described by Van Waerbeke et al. (1997), the ACF allows a maximum use of the signal which increases significantly the signal-to-noise ratio on the measurement of the local shear. Ideally, all the pixels of the images could be used, but in practice we experienced that a better signal-to-noise ratio can be achieved if the ACF is computed on restricted areas centered around each galaxy, previously detected by a standard technique. The main reason for this is that, as suggested from the deep HDF image, even at extremely faint magnitude, a large fraction of the CCD frames remains free from very faint sources, showing that the faint-end

slope of the galaxy number counts decrease substantially and cannot provide a complete coverage of the whole field with faint galaxies, down to the confusion limit. This fact limits the efficiency of the ACF in ‘empty regions’ of the CCD since only a low signal is coming from background sources hidden in the noise. In addition, as we shall see further below, the data acquisition and the pre-processing procedures (shift-and-add) as well as the electronic boards of the CCD camera generate correlated residual noise which perturb the measurement of the ellipticities of very faint galaxy images. We therefore decided to optimize the algorithm by using first SExtractor for source detection, and then by applying the ACF around those sources only. The efficiency of this method has been discussed already by Van Waerbeke & Mellier (1997).

In this Section we focus on the results from the ACF method and the comparison with the SExtractor measure using exactly the same galaxies. Furthermore we will compare these results with the previous BM analysis.

For each field, a new SExtractor catalogue has been built using standard but different selection criteria than the previous analysis. Typically the convolution filter is larger and does not permit the detection of faint peaked objects.

The catalogues contain $N_g = 145$ galaxies for PKS1508, $N_g = 129$ for PKS0135 and $N_g = 181$ for 3C446. Only objects with FLAG=0 are kept, to be sure to eliminate all the possible external source of distortion, and the magnitude ranges are [22, 28], [21.3, 27.3], and [22.3, 28.3]. These restrictive conditions explain why the number of galaxies is slightly smaller than in the BM catalogues. As a first step, the mean ellipticity was calculated in the whole fields. Since the seeing on these fields ranges from 0''.66 to 0''.76, this corresponds to a gaussian PSF of size 5 to 6 pixels in the ACF space. This means that, ideally, we have to use an isophotal annular filter of mean diameter equal to 6 pixels to compute the shape parameters of the ACF. In Figs. 8 through 10, the ACFs for the three QSO fields are shown. These figures reveal the fact that the ACF’s center is polluted by an instrumental small-scale pixel-pixel correlation probably due to the reasons discussed above. To avoid this center we used an annular filter with 10 pixels diameter, larger than the ideal filter size. The inconvenience is that at larger distance from the ACF’s center, the S/N is lower. The ellipticities are computed in different magnitude bins. The results are shown in Figs. 5 through 7. The shear detection in PKS1508 is robust and confirms the results of Sect. 3. The other two field do not show a significant distortion, although a significant shear is detected in the field of PKS0135 if only the brighter galaxies are used. The agreement between SExtractor and ACF is very good. However, it seems that at magnitudes fainter than 27 the ACF measures a larger signal. In fact, because for the faintest galaxies, the instrumental structure in the ACF (Figs. 8 through 10) becomes important, the measurement is not accurate. To see how this instrumental effect alters the ellipticity measurement, Fig. 11 shows the same ellipticity as Fig. 5, but using an annular filter closer to the ACF center, with a diameter of 6 pixels. The anomalously high value of the ellipticity is clear, and is due to the fact that the instrumental distortion is in the same direction as the ellipticity orientation. Only a large diameter for the filter and/or the use of the brighter galaxies only allows to avoid this problem.

The measurements were performed in the whole field T and in the subfields ABCD using a more restrictive condition on the magnitude of the objects. The objects are brighter than a threshold magnitude m_{lim} . The results are shown on Tables 4 through 6. The number of galaxies is significantly smaller than in the Tables 1, 2 & 3 for the BM

analysis because of our more restrictive detection conditions here. While the ACF and SExtractor results are consistent, it is difficult to compare them with BM in the ABCD fields because the galaxy samples are different. However, in the T fields, the number of galaxies is large and the results are consistent. The detection of the shear in PKS1508 is confirmed. It was impossible to performed the calculations in the subfields 1-9 because of the very small number of galaxies. We note that some subfields (D in PKS1508 and C in PKS0135) show a large value of the shear, with a significance level of $4.2\sigma^1$ and 2.8σ , respectively, with the ACF. An interesting point is the 2.9σ detection of an homogeneous shear in the whole field of PKS0135, if only the brightest galaxies ($m_{\text{lim}} = 23.5$) are kept.

Since it is difficult to compare with the BM results, because the selection criteria are not *exactly* the same, we decided to perform an additional analysis which consists of using the three methods on a set of galaxies which are present in the three catalogues. For each field, the resulting catalogue corresponds to highly conservative selection criteria. The number of objects are, respectively, 93, 73 and 128 for the PKS1508, PKS0135, and 3C446 fields. The BM ellipticities are recalibrated with SExtractor ellipticities. We find that the calibration constants C are changed compared to Sect. 3, which demonstrates that this calibration depends on the magnitude of the galaxies, which is not surprising. The results are shown in Tables 7, 8, 9. The agreement between the methods is remarkable, and confirms the detection of a cosmic shear in PKS1508. The polar coordinates of the shear ($|\epsilon|, \theta$) are also displayed for easier visualisation of the geometry of the distortion. The small excess in the intensity measured by the ACF compared to SExtractor is probably due to the fact that SExtractor measures the image brightness moments only from those pixels above a given flux threshold. This confirms the results obtained from simulated images (Van Waerbeke 1997).

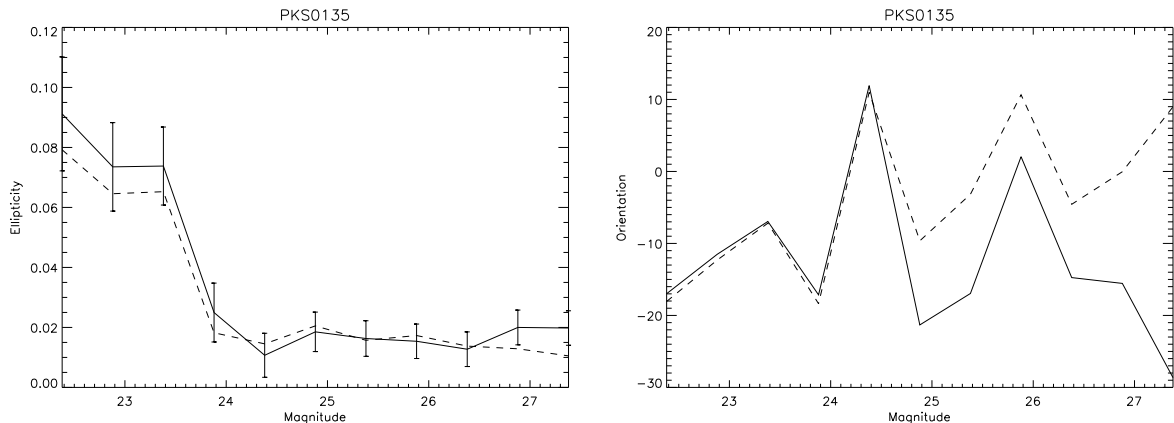


Fig. 5. In the left panel, the value of the mean ellipticity of the shear in PKS0135 as a function of the upper bound value m_{lim} of the magnitude interval is plotted. The right panel shows the orientation angle of the mean ellipticity. The solid curves correspond to the ACF, and the dashed curves to the SExtractor results. The errors bars are the 1σ intervals due to the intrinsic ellipticities of the galaxies; note that the decrease of the size of the error bars due to the increase in galaxy number with fainter magnitude is partly compensated by increases ellipticities of galaxy images, which is mainly due to the increasing noise.

¹ Here, the significance level is determined from the random intrinsic ellipticity of the galaxies, which is very close to the rms ellipticity of the observed images.

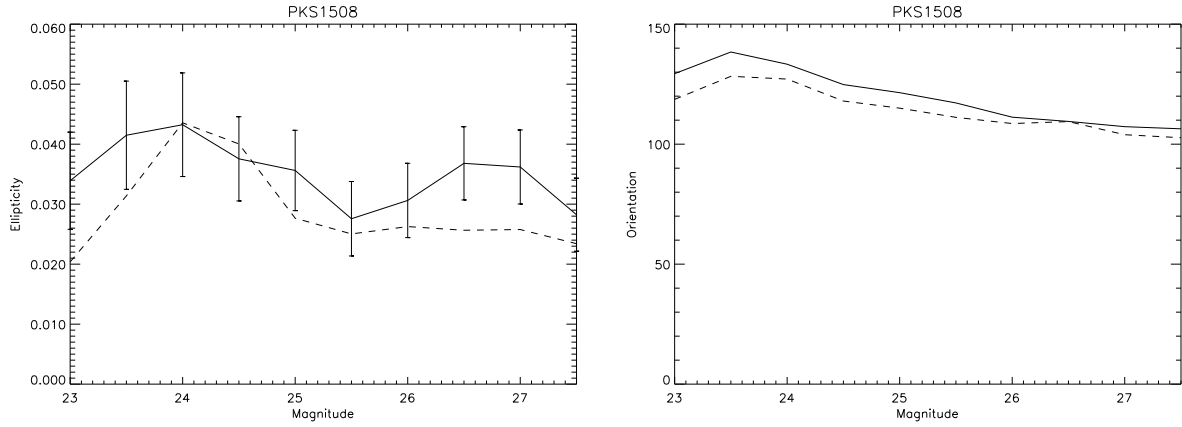


Fig. 6. Same as Fig. 5 for the PKS1508 field

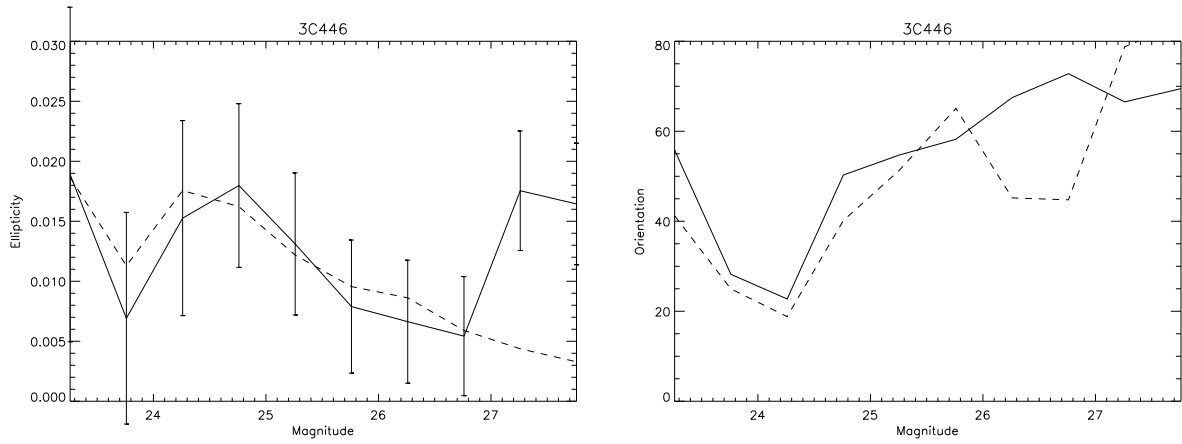


Fig. 7. Same as Fig. 5 for the 3C446 field

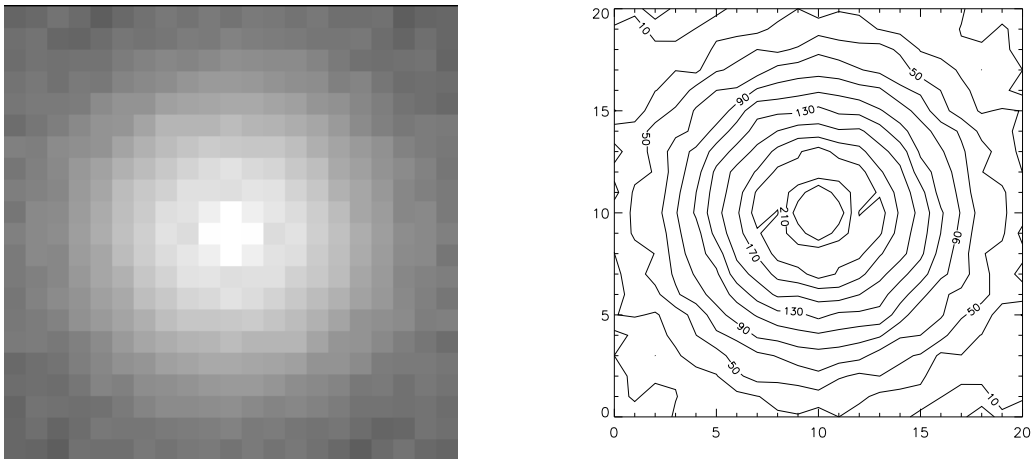


Fig. 8. The left panel shows the ACF of the faint galaxies ($m \in [21.3, 27.3]$) in the field PKS0135. The central structure is probably due to correlated pixel-to-pixel noise due to CCD read-out and data reduction processes. On the right, the contour levels show this internal structure and the regularity of the ACF's isophotes.

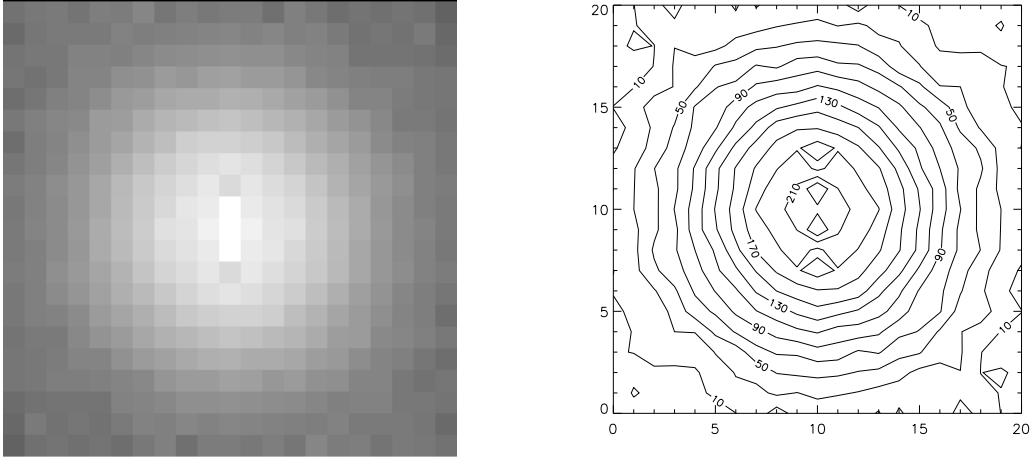


Fig. 9. Same as Fig. 8 for the PKS1508 field. The magnitude range is $m \in [22, 28]$.

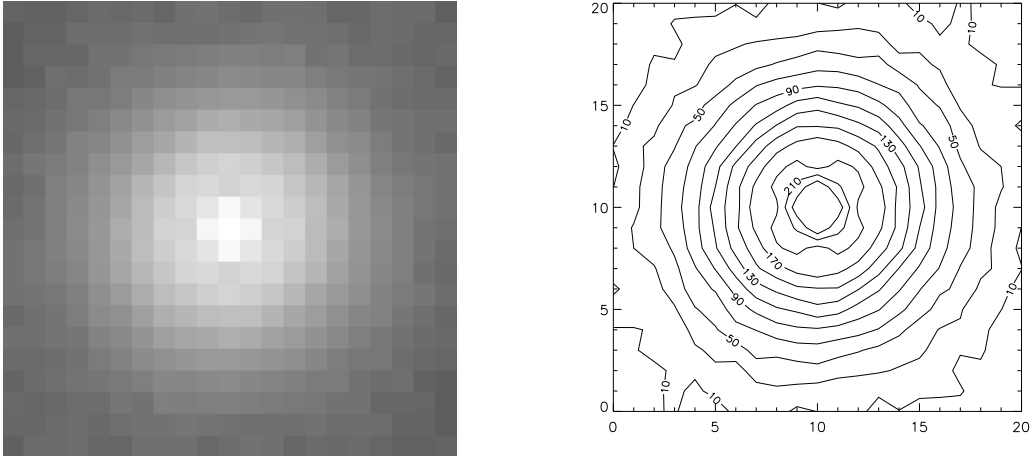


Fig. 10. Same as Fig. 8 for the 3C446 field. The magnitude range is $m \in [22.3, 28.3]$.

Table 4. For the QSO 0135 and the TABCD (sub)fields as described in the text, the number N of objects, and the measured mean ACF ellipticity is compared to the S-ellipticity. The upper magnitude limit is $m_{\text{lim}} = 25.3$

(Sub)field	N	ϵ_1^{ACF}	ϵ_2^{ACF}	ϵ_1^{S}	ϵ_2^{S}
T	81	1.35	-0.91	1.55	-0.17
A	19	0.98	0.56	2.94	-0.02
B	23	-0.52	-0.53	-0.81	0.14
C	24	5.16	-2.98	3.41	-1.81
D	15	-1.34	0.14	0.69	1.70

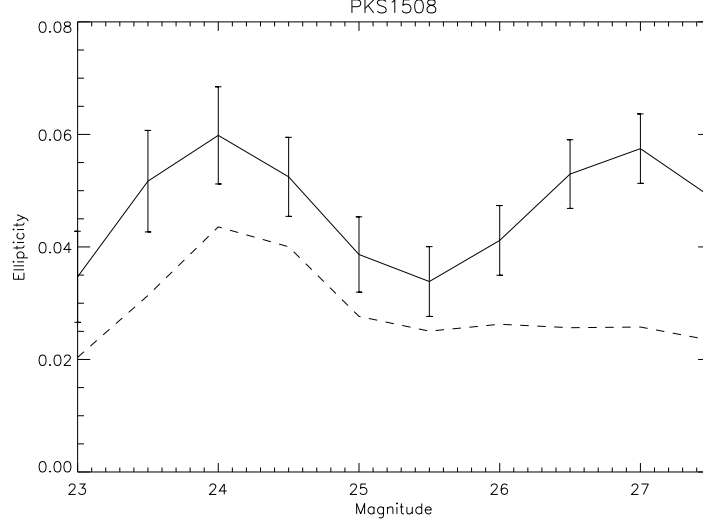


Fig. 11. Same as Fig. 6, but with a smaller annular isophotal filter. The larger value of the shear compared to Fig. 6 in the ACF method is due to the internal structure showed on Fig. 9

Table 5. For the QSO 1508 and the TABCD (sub)fields as described in the text, the number N of objects, and the measured mean ACF-ellipticity is compared to the S-ellipticity. The upper magnitude limit is $m_{\text{lim}} = 26$.

(Sub)field	N	ϵ_1^{ACF}	ϵ_2^{ACF}	ϵ_1^{S}	ϵ_2^{S}
T	118	-2.26	-2.03	-2.09	-1.59
A	33	-3.80	0.08	-3.38	0.09
B	28	-3.00	-0.56	-1.84	-1.15
C	25	-2.46	0.20	-1.94	-0.51
D	32	0.61	-7.76	-1.14	-4.61

Table 6. For the QSO 3C446 and the TABCD (sub)fields as described in the text, the number N of objects, and the measured mean ACF-ellipticity is compared to the S-ellipticity. The upper magnitude limit is $m_{\text{lim}} = 26.2$

(Sub)field	N	ϵ_1^{ACF}	ϵ_2^{ACF}	ϵ_1^{S}	ϵ_2^{S}
T	140	-0.46	0.48	-0.06	0.86
A	43	0.82	2.25	0.34	1.91
B	27	-1.63	-1.47	2.24	-0.52
C	34	-0.63	2.71	-0.38	2.91
D	36	-0.92	-2.84	-1.78	-1.20

Table 7. Comparison of the 3 methods used in this paper (ACF, BM, and SExtractor) for PKS0135 using the whole image. A total of 73 objects are kept, only those which are common to the 3 catalogues and with FLAG=0. The limiting magnitude here is $m_{\text{lim}} = 25.3$. The quantity $(|\epsilon|, \theta)$ is the mean ellipticity and mean orientation.

Methods	ϵ_1	ϵ_2	$ \epsilon $	θ
ACF	1.43	-0.89	1.68	-16
BM	1.37	0.42	1.43	8
Sex	1.26	-0.68	1.43	-14

Table 8. Same as Table 7, for PKS1508, with 93 objects, and $m_{\text{lim}} = 26$.

Methods	ϵ_1	ϵ_2	$ \epsilon $	θ
ACF	-2.28	-3.62	4.28	119
BM	-2.83	-2.53	3.80	111
Sex	-2.58	-2.78	3.80	114

Table 9. Same as Table 7 for 3C446 128 objects, and $m_{\text{lim}} = 26.3$.

Methods	ϵ_1	ϵ_2	$ \epsilon $	θ
ACF	-1.30	1.15	1.74	69
BM	-1.11	0.97	1.47	69
Sex	-1.00	1.09	1.47	66

5. The two-point correlation function of the galaxy ellipticities

We have analyzed the mean shear present in the three QSO fields in sections 3 and 4. The fields were subdivided and the mean shear in sub-fields was compared, and its significance tested by randomizing the ellipticity position angles to generate mock data. In this section we analyze the data in a somewhat complementary way by computing the ellipticity auto-correlation function defined as

$$C_{\epsilon\epsilon}(\theta) = \langle \epsilon(\varphi) \epsilon^*(\varphi + \theta) \rangle_{\varphi}, \quad (2)$$

where the angular brackets denote ensemble averaging. For a finite set of data it is evaluated by considering all pairs available with angular separation in a small interval around $\theta = |\theta|$. Note that the correlation function C_{pp} defined in Jain & Seljak (1996) uses an ellipticity estimate which for small ellipticities is twice as large as ϵ , and so $C_{pp}(\theta) = 4C_{\epsilon\epsilon}(\theta)$; for notational consistency, we shall use $C_{\epsilon\epsilon}$ henceforth. While $C_{\epsilon\epsilon}$ does not retain any information about the location of the galaxies, it highlights the relative contributions to the mean shear from correlations on different angular scales. It is also a convenient statistic to compare with theoretical predictions. As discussed below, ideally one would like at least 10 well separated fields to get a sensible measurement of $C_{\epsilon\epsilon}$ for comparison with theoretical predictions. For just one field, it is more useful as a complementary check of the robustness of the signal and a test of approximate quantitative agreement with predictions.

We typically have about 150 galaxies in fields of $2'$ on a side. We compute $C_{\epsilon\epsilon}$ by binning pairs into 5 bins logarithmically spaced in θ . Each bin, except for the first, has over 2000 pairs of BM ellipticities which we average over to compute $C_{\epsilon\epsilon}$ as defined in Eq.(2). We found that for the fields of QSO 3C446 and PKS0135, the data did not provide a non-zero $C_{\epsilon\epsilon}$ that was robust to resampling and small variation of the bin size. For the field of PKS1508 however, we measure a robust, non-zero value of $C_{\epsilon\epsilon}$ for 3 of the 5 angular bins.

The results for PKS1508 are shown in Figure 12 which shows $C_{\epsilon\epsilon}(\theta)$ vs. θ in arcminutes. The solid error bars are the $1\text{-}\sigma$ deviations obtained from bootstrap resampling of the data. A closer examination of the distribution of the bootstrap resampled $C_{\epsilon\epsilon}$'s showed a positively skewed distribution. The true error bars are therefore shifted slightly upward from what is shown, thus providing a firmer lower limit. The detected value of

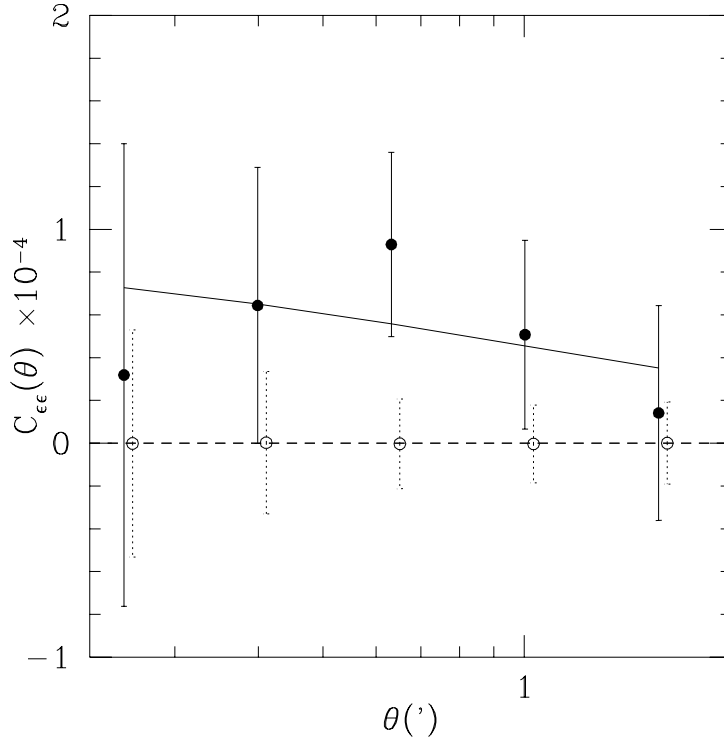


Fig. 12. $C_{ee}(\theta)$ computed using the Bonnet-Mellier ellipticities for the field of PKS1508 (filled dots), plotted vs. θ in arcminutes. The solid error bars are the 1- σ bootstrap resampling deviations. The circles and the dashed error bars (slightly displaced in θ for clarity) show $C_{ee}(\theta)$ computed for simulated data obtained by randomizing the position angles of the measured galaxy ellipticities, and the corresponding 1- σ deviations for 10,000 such data sets. The solid curve is the fit $C_{ee} = a/(\theta + 1')$ to the measured data (see text for details).

C_{ee} is above the 1- σ level for 3 of the bins, and for the central bin centered on $0'.62$ it is above the 2- σ level.

The robustness of the detection of a non-zero C_{ee} can be further tested by randomizing the position angles of the measured galaxy ellipticities as before. 10,000 such simulated data sets were used to obtain the results shown as circles and dashed error bars in Figure 88. The result as expected is a zero average value of C_{ee} ; more useful are the size of the error bars which provide an alternative estimate of the significance level of the values plotted in the left panel. We found that less than 0.4% of the simulated data yielded a value of C_{ee} greater than or equal to the value measured from the data at $\theta = 0'.62$. The (dashed) error bars obtained from randomizing the orientations of galaxies are more relevant for the statistical significance for the deviation of C_{ee} from that expected for a random ellipticity distribution.

Theoretical cosmological models, normalized empirically (to the abundance of rich galaxy clusters, following White et al. 1993) predict a value of C_{ee} for $\theta = 1'$ of about 5×10^{-4} for reasonable values of Ω and Λ (Jain & Seljak 1996). COBE-normalized models tend to predict higher C_{ee} , so that an upper limit for $C_{ee}(\theta = 1') \simeq 1.2 \times 10^{-3}$ is reasonable. Larger values would severely conflict with data from large-scale structure and other studies. For CDM-like models, C_{ee} varies as $1/\theta$ for $\theta > 1'$ and approaches a

constant for θ much smaller than $1'$.

With this theoretical bias in mind, we fitted a function of the form $a/(1' + \theta)$, with the amplitude a fitted from the measured $C_{\epsilon\epsilon}$. The measured values in the 5 bins were combined, inversely weighted by the variance, to get a best fit value for a . We obtained the result $a = 0.91 \times 10^{-4}$, and found that fewer than 0.4% of the randomized samples yielded a value of a larger than this value; this fit is also plotted in Fig. 12. It should be noted that this functional form does not fit very well to the measured data points; by using a somewhat more complicated shape of the fit function, a higher significance can be obtained, but we have not tried this fine-tuning.

In order to compare the amplitude of the measured $C_{\epsilon\epsilon}$ with the theoretical results we must correct the Bonnet-Mellier ellipticities to estimate the true $C_{\epsilon\epsilon}$. Since the correction factor is approximately 5, we obtain $a_{\text{corrected}} \simeq 0.002$, or $C_{\epsilon\epsilon}(1') \simeq 10^{-3}$ which is close to the upper limit of the theoretical prediction. While a single field of view $2'$ on a side is too small to draw quantitative conclusions from, it is interesting that the measured values of $C_{\epsilon\epsilon}$ are within the range of theoretical predictions.

6. Discussion and conclusions

Using various methods, we have shown that the shear found in FMDBK around at least one high-redshift QSO is statistically highly significant. Whereas the significance of the shear over the full fields of PKS0135–247 and 3C446 is not very high, the probability to find a shear in excess of that seen in PKS1508–05 from a randomly oriented sample of galaxy images is below 0.4%, as demonstrated by several methods. The main reason for this high level of significance is the remarkable circularity of the PSF as measured from isolated stellar objects in the SUSI fields. Moreover the residual anisotropy of the PSF in the field of PKS1508–05, of order 1%, was shown to be oriented perpendicular to the mean ellipticity of galaxy images and therefore cannot cause the observed statistical alignment. The shear in the field of QSO Q1622+236, where FMDBK also found a significant signal, was not considered in the present paper as it was observed with a different telescope.

For the interpretation of the statistically significant shear in the field of PKS1508–05 one has to consider the field selection employed by FMDBK. Their main motivation was to test the hypothesis put forward by Bartelmann & Schneider (1992) that the observed associations of foreground galaxies with high-redshift QSOs on arcminute scales is due to lensing by the large-scale structure in which the galaxies are embedded, and thus overdense in regions of high magnification by lensing. Therefore, FMDBK have selected several high-redshift QSOs with large flux in both optical and radio wavebands. If the Bartelmann & Schneider hypothesis is true, then the lines-of-sight selected by FMDBK are biased for the presence of a lensing effect.

We therefore discuss three alternative interpretations of the detected signal:

(1) The first is to assume that the QSO-galaxy associations on arcminute scales is a statistical fluke, or that it is unrelated to gravitational lensing. Given the increasing evidence for such correlations (e.g., Bartelmann & Schneider 1994 and references therein; Benítez & Martínez-González 1997), we consider these alternatives unlikely as there appears no plausible alternative to lensing to explain the correlations. Nevertheless, if we discard the lensing interpretation, then the lines-of-sight to the QSOs would be

unbiased, and the shear in PKS1508–05 would be the first detection of ‘cosmic shear’ along an unbiased line-of-sight.

One has to be careful at this point to clarify the meaning of ‘cosmic shear’. In the early work on this subject (e.g., Blandford et al. 1991; Kaiser 1992), the linear evolution of the power spectrum was considered, and the ‘cosmic shear’ considered was solely due to the diffuse, large-scale matter distribution. It was predicted to be coherent over scales below one degree and to have an rms value on arcminute scales of about 1%, depending on the cosmological model. These estimates were revised upwards by considering the fully non-linear evolution of the power spectrum (Jain & Seljak 1996), predicting an rms shear on scales of a few arcminutes of a few percent. It is unclear at the moment whether the rms shear on these scales is dominated by fairly large, slightly non-linear density concentrations, or by fully non-linear collapsed objects like clusters. In the second case, the shear field around clusters would have to be included as part of ‘cosmic shear’ as well, though a cluster field would constitute a strongly biased line-of-sight. The detection of a significant shear in the field of PKS1508–05 would then still be exciting because this would be the first detection of coherent shear in a direction not targeted towards a known mass concentration.

(2) If the QSOs are indeed magnification biased, the mass responsible for the observed shear may be related to the mass magnifying the QSOs. In that case, the detection of cosmic shear in the field of PKS1508–05 would not be along an unbiased direction, but still not targeted towards a known mass concentration. The detected shear would then support the magnification bias hypothesis. The true cosmic shear amplitude would probably be smaller than the value measured by us.

(3) The shear is caused by material physically associated with the QSO PKS1508 ($z = 1.19$). This would imply that the faint galaxies have a high-redshift tail which is not implausible, given that the high redshift cluster MS1054 ($z = 0.83$) shows a clear weak lensing signal (Luppino & Kaiser 1997; see also Deltorn et al. 1997), and also from the number density depletion in the cluster 0024+16 (Fort, Mellier & Dantel-Fort 1996). In that case the shear in the field of PKS1508 would be analogous to the one in the field of 3C324 (Smail & Dickinson 1996). However, the observations in the field of 3C324 went to considerably fainter magnitudes and thus presumably higher mean redshifts of the galaxies. Also, the shear pattern in PKS1508 seems to be quite uniform, whereas in 3C324 a systematic tangential alignment relative to the radio source is seen. We therefore consider material associated with the QSO to be an unlikely candidate for producing the observed shear.

In the field of PKS1508, the shear amplitude on a scale of $1'$ is about 3%, and thus in approximate agreement with theoretical expectations. However, our results do not allow for any quantitative cosmological interpretation for two principal reasons. First, if one considers the possibility (2) as the most likely one, the shear was measured along a biased line-of-sight and may therefore not be representative of a random line-of-sight. Second, in order to draw any conclusion from cosmic shear measurements, several uncorrelated lines-of-sight have to be observed (e.g., Kaiser 1996). In the near future measurements along unbiased lines-of-sight with much larger fields of view will be possible. The key factor in obtaining quantitative results on weak lensing will be the control of systematic distortions in the instruments. Our results demonstrate that the stability of the PSF of the SUSI camera across its field could compensate for the relatively small size of the field by providing shear measurements of very high significance.

Acknowledgements

This work was supported by the “Sonderforschungsbereich 375-95 für Astro–Teilchenphysik” der Deutschen Forschungsgemeinschaft and by the Programme National de Cosmologie of the Centre National de la Recherche Scientifique in France. We thank S.D.M. White for carefully reading the manuscript.

References

- Bartelmann, M. 1995, A&A 298, 661.
- Bartelmann, M. & Schneider, P. 1992, A&A 259, 413.
- Bartelmann, M. & Schneider, P. 1994, A&A 284, 1.
- Benítez, N. & Martínez-González, E. 1997, ApJ 477, 27.
- Bernardeau, F., van Waerbeke, L. & Mellier, Y. 1996, A&A *in press*, astro-ph/9609122.
- Bertin, E. 1996, PhD Thesis. Université Paris VI.
- Bertin, E. & Arnouts, S. 1996, A&AS 117, 393.
- Blandford, R.D., Saust, A.B., Brainerd, T.G. & Villumsen, J.V. 1991, MNRAS 251, 600.
- Bonnet, H. & Mellier, Y. 1995, A&A 303, 331.
- Bower, R. & Smail, I. 1997. Preprint astro-ph/9612151.
- Deltorn, J.-M., Le Fèvre, O., Crampton, D. & Dickinson, M. 1997, astro-ph/9704086.
- Fahlman, G., Kaiser, N., Squires, G. & Woods, D. 1994, ApJ 437, 56.
- Fort, B. & Mellier, Y. 1994, A&AR 5, 239.
- Fort, B., Mellier, Y., Dantel-Fort, M., Bonnet, H. & Kneib, J.-P. 1996, A&A 310, 705 (FMDBK).
- Fort, B., Mellier, Y. & Dantel-Fort, M. 1996, astro-ph/9606039.
- Jain, B. & Seljak, U. 1996, astro-ph/9611077.
- Kaiser, N. 1992, ApJ 388, 272.
- Kaiser, N. 1996, astro-ph/9610120.
- Kaiser, N. & Squires, G. 1993, ApJ 404, 441.
- Kaiser, N., Squires, G. & Broadhurst, T. 1995, ApJ 449, 460.
- Luppino, G. & Kaiser, N. 1997, ApJ 475, 20.
- Miralda-Escudé, J. 1991, ApJ 380, 1.
- Mould, J. et al. 1994, MNRAS 271, 31.
- Narayan, R. & Bartelmann, M. 1996, astro-ph/9606001.
- Schneider, P. 1996, in: *The universe at high-z, large-scale structure and the cosmic microwave background*, Proceedings of an advanced summer school, Laredo, Cantabria, Spain, eds. E. Martínez-Gonzales and J.L. Sanz, Lecture Notes in Physics 470, Springer-Verlag, p. 148.
- Seitz, C., Kneib, J.-P., Schneider, P. & Seitz, S. 1996, A&A 314, 707.
- Smail, I. & Dickinson, M. 1995, ApJ 455, L99.
- Squires, G. et al. 1996, ApJ 461, 572.
- Steidel, C., Dickinson, M., Meyer, D., Adelberger, K. & Sembach, K. 1996, astro-ph/9610230.
- Tyson, J.A. 1986, AJ 92, 691.

- van Waerbeke, L. 1997 PhD Thesis Université Paris XI Orsay
- van Waerbeke, L., Mellier, Y., Schneider, P., Fort, B. & Mathez, G. 1997, *A&A* 317, 303.
- van Waerbeke, L. & Mellier, Y. 1997, proceedings of the XXXIèmes Rencontres de Blois.
Les Arc. astro-ph/9606100.
- Villumsen, J. 1996a, *MNRAS* 281, 369.
- Villumsen, J. 1996b, *MNRAS*, submitted.
- White, S.D.M., Navarro, J.F., Evrard, A.E. & Frenk, C.S. 1993, *Nat* 366, 429.
- Wilson, G., Cole, S. & Frenk, C.S. 1996, *MNRAS* 280, 199.